Mechanical properties of composite structures

MSE 340 Composites - travaux pratiques 2022

MED 3 1523

jialiang.fan@epfl.ch

1 Introduction

Mechanical properties of composite materials can be assessed using a wide variety of tests such as tensile, compressive, shearing, or bending tests. These tests enable the determination of intrinsic properties, the evaluation of anisotropies by measuring the different stiffness moduli and Poisson ratios as well as the evaluation of the structural stiffness which depends also on the specimen geometry.

The objective of this TP is to perform selected mechanical tests to study the mechanical behaviour of different types of composite materials and structures:

- *Flexural stiffness using a three point bending test*

  Materials tested will be a laminate of epoxy resin reinforced by glass fibre fabrics, and sandwich structures produced using this laminate for the skin layers and several other materials for the core. The principle of a sandwich structure is to have a lightweight core material between two skin layers, as this construction yields a structure that exhibits a much higher stiffness but the same mass as the skin alone.

- *Mode I energy release rate using a double cantilever beam (DCB) test*

  The material tested will be a laminate of epoxy resin reinforced with a stack of 16 glass fiber twill weave plies. The fracture of composites and laminates occurs mainly by delamination of the laminate plies. Furthermore, breakage is influenced by the type of the reinforcement phase (unidirectional fibres, fabrics, mats, and so on). To characterize the delamination resistance, the principles of linear mechanics of a beam stressed in mode I fracture can be used.

2 Theory

2.1 Flexural stiffness of composite beams

According to the Euler-Bernouilli beam theory, the maximum deflection of a simply supported beam loaded in a three point bending configuration occurs at its centre. The deflected distance δ is directly proportional to the load P, and depends on the test configuration (distance between supports L) and the beam's materials properties (elastic modulus E) and geometry (second moment of area of the beam's cross-section I):

$$\delta = \frac{L^3}{48EI}P \tag{1}$$

The flexural stiffness of a beam D is then defined as the product of the elastic modulus E and the second moment of area I:

$$D = EI \tag{2}$$

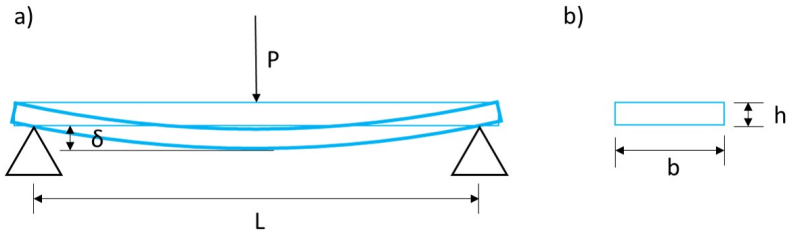

Figure 1: a) Three point bending test showing the applied load P, the span L and the deflection of a beam δ, and b) rectangular cross section of the beam, iwth height h and width b.

For a beam with a rectangular cross-section of height h and width b such as the one depicted in figure 1, the value of the second moment of area is $I = \frac{bh^3}{12}$, and therefore equations 1 and 2 can be rewritten as:

$$\delta = \frac{L^3}{4Ebh^3}P \tag{3}$$

$$D = E\frac{bh^3}{12} \tag{4}$$

In the case of a sandwich structure with the cross sectional geometry depicted in figure 2, the total flexural stiffness will be the sum of the flexural stiffnesses of the outer skins D_s and the core D_c:

$$D = 2D_s + D_c = 2E_sI_s + E_cI_c = E_s\left(\frac{bt^3}{6} + \frac{btd^2}{2}\right) + E_c\frac{bc^3}{12} \tag{5}$$

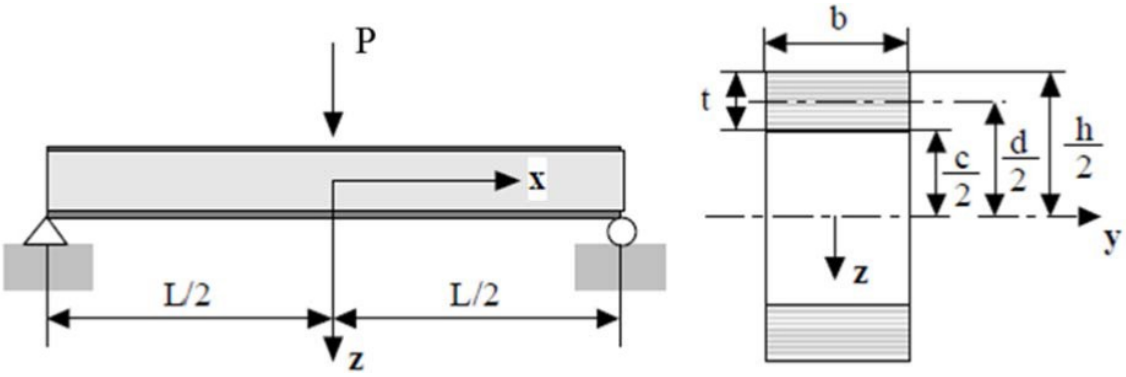

Figure 2: a) Three point bending test and geometry of a sandwich beam, including the span L, the load P, the skin thickness t, the core thickness c, the height h and width b, and the geometrical quantity d, which corresponds to the core + one skin thickness.

where E_s and E_c are the elastic moduli of the skin and core respectively.

If we consider that the skin thickness is negligible and that the core elastic modulus is small compared to the skin one, then equation 5 can be approximated by:

$$D \approx E_s \frac{btd^2}{2} \tag{6}$$

However, the classical Euler-Bernouilli deflection falls short when applied to sandwich beams, and equations 1 and 3 become insufficient to describe their mechanical behaviour in a three point bending test. In order to correct the total deflection, the shear deformation of the beam must also be taken into account, as shown in figure 3. To a first approximation, we can assume that the bulk of the shear will be bore by the core, and the total deflection of the sandwich can be rewritten as:

$$\delta = \frac{L^3}{48D}P + \frac{L}{4S}P \tag{7}$$

where $D \approx E_s \frac{btd^2}{2}$ is the flexural stiffness of the beam and $S = G_c \frac{bd^2}{c}$ is its shear stiffness, which depends on the shear modulus of the core G_c.

2.2 Delamination of composites

In a composite structure, fracture properties are significantly determined by the nature of the adhesion between the fibres and the matrix. This can lead to various failure modes such as debonding, fiber or matrix rupture, or delamination. Some of the main events that occur during composite damage can be observed in figure 4. Delamination tests offer a good way to characterize the damage caused by fatigue or impact.

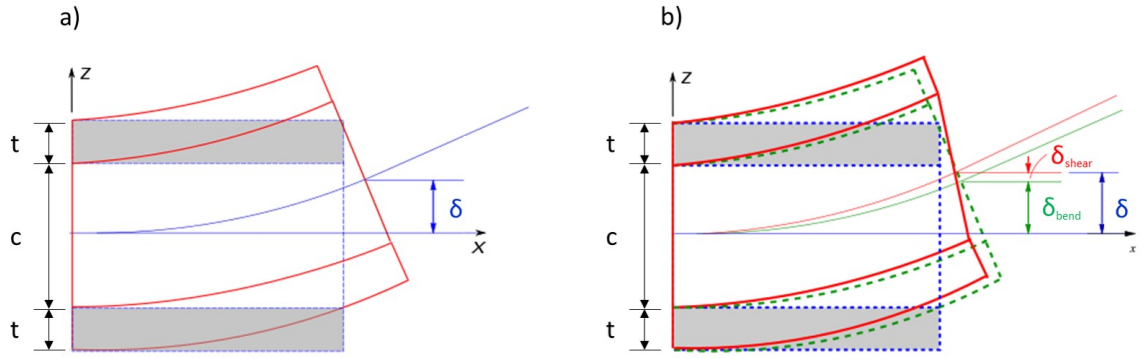

Figure 3: a) Classical Euler-Bernouilli deflection of a sandwich beam, and b) shear-corrected deflection of a sandwich beam, depicting the amount due to bending δ_{bend} and shear δ_{shear}.

Two interdependent approaches exist in the context of linear fracture mechanics to study crack propagation in materials: the energy approach (energy release rate G) and the local stress field approach (stress concentration factor K).

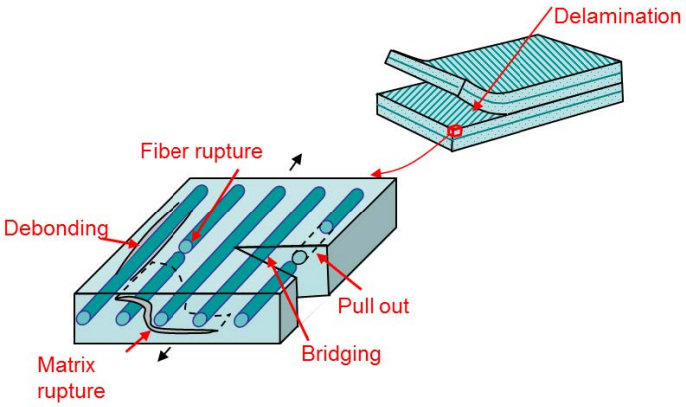

Figure 4: Different modes of composite damage.

In the energy approach the propagation of a crack in a stressed, homogeneous and elastic material is thermodynamically possible. According to Irwin's criterion, the energy release rate G is defined as the negative variation in potential elastic energy U_{el} with respect to crack area A:

$$G = -\frac{dU_{el}}{dA} \tag{8}$$

If we consider a slab of material with thickness B containing an edge crack of length a and loaded with a force P that produces a displacement δ such as the one depicted in figure

5, the energy release rate can be rewritten as:

$$G = -\frac{dU_{el}}{dA} = -\frac{d}{d(Ba)}\left(-\frac{1}{2}P\delta\right) = \frac{P}{2B}\frac{d\delta}{da} \tag{9}$$

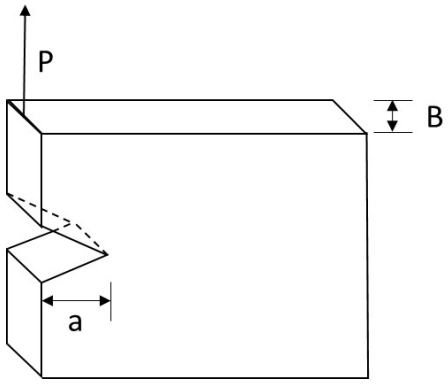

Figure 5: Diagram for propagation of an edge crack.

Generally speaking, crack propagation occurs if the reduction of elastic energy caused by the relaxation of the material is at least infinitesimally larger than the energy dissipated in other processes (creation of new crack surfaces, plastic deformation, viscoelastic effects, and so on). In the context of linear fracture mechanics, this means that the energy release rate needs to be greater than the material's resistance to crack extension R:

$$G \geq R \tag{10}$$

Furthermore, crack propagation can happen in a stable or unstable fashion depending on the variation of G and R with the crack extension:

$$\begin{aligned} \frac{dG}{da} &< \frac{dR}{da} \Rightarrow \text{stable crack propagation} \\ \frac{dG}{da} &\geq \frac{dR}{da} \Rightarrow \text{unstable crack propagation} \end{aligned} \tag{11}$$

Stable crack propagation is minimal in brittle materials such as ceramics that undergo little or no plastic deformation, and such materials catastrophically break in an unstable fashion when the energy release rate reaches a critical value G_c, which occurs for a critical crack length a_c as per Griffith's theory. On the other hand, metals and composites allow for stable and steady propagation of cracks with lengths smaller than a_c, above which they also break in an unstable fashion.

2.2.1 Mode I fracture

The analysis of delamination of a composite material in mode I can be illustrated by the behaviour of a beam in bending:

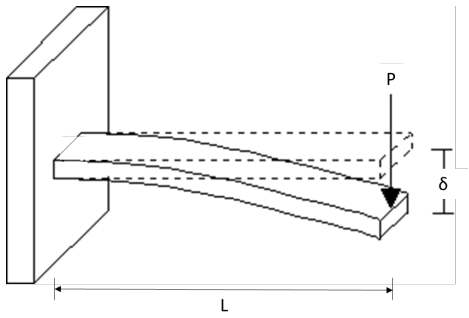

Figure 6: Bending of a cantilever beam of length L with a load P produces a deflection δ.

Due to the anisotropic nature of many composites (matrix + reinforcement), the original Euler-Bernouilli solution for a cantilever beam can be adapted to include the effects of shear and rotation by using an exponent n, and therefore the deflection δ can be written as:

$$\delta = \frac{L^n}{3EI}P \tag{12}$$

where P is the applied load, EI the flexural stiffness of the beam and L is its length. In a delamination experiment (for example with a double cantilever beam configuration), the crack length a is equivalent to the length L in equation 12, and we can therefore calculate the energy release rate using equations 9 and 12:

$$\frac{d\delta}{da} = n\frac{a^{n-1}}{3EI}P = n\frac{\delta}{a} \Rightarrow G_I = \frac{nP\delta}{2aB} \tag{13}$$

2.2.2 Mode II fracture

In reality, the breakage of a composite due to delamination is often accompanied by shear failure (mode II). According to the beam theory, a bending load causes a maximum shear stress in the neutral fibre of the beam, while the tension and compression stresses are zero. Thus, a beam (pre-cracked in the neutral fibre) has to be loaded in bending to obtain a pure mode II loading.

3 Experiments

3.1 Three-point bending test of sandwiches

The composite structures tested in this part of the TP are made of laminates of an epoxy resin reinforced by glass fibre fabrics, and prepared by contact moulding. For the sandwich

structure, there are four different core materials available: balsa wood, Nomex, PVC and crosslinked PEI. The interface between core and skin is made of epoxy.

The tests are performed on the tensile testing machine UTS, using the configuration 'three-point bending'. To avoid damaging the structure, the beam is deformed only elastically. During each test the load P is recorded as a function of the beam deflection δ, whereby the beam deflection corresponds to the displacement of the traverse of the machine.

The purpose of the three-point bending test is to study the mechanical behaviour of the different beams. In the first part, the composite laminate and the sandwich will be tested using a fixed span L. In the second part, a sandwich will be selected and tested for different spans.

3.2 Mode I delamination test

For the delamination tests, the UTS is used as well. The principle of the DCB (double cantilever beam) mode I is illustrated in the following figure:

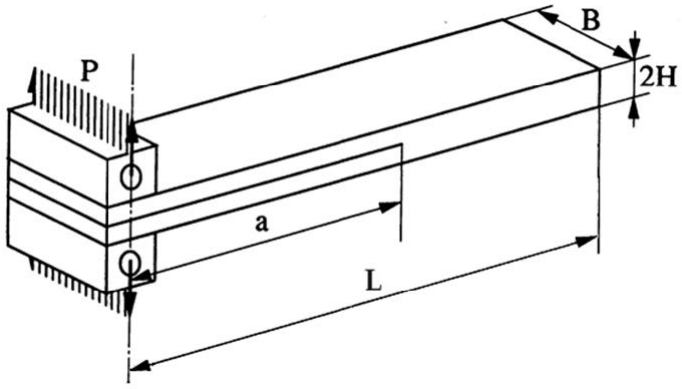

Figure 7: Configuration of the delamination test in mode I, with applied load P, crack length a, beam length L, width B, and height $2H$.

This standardised test is performed on a laminate sample produced by contact moulding. The pre-crack of length a_0 is thereby obtained by inserting two non-adherent foils (one of each side of the crack) in the composite beam during fabrication. To be able to clamp the laminate in that way that the crack can open and thus grow along the interface of two fabric layers during the test, two pins are glued on the surface of the beam end with crack. The chosen strain rate is 5 mm/min.

The fracture energy is determined by the calculation of the crack advancement for each point. Therefore, the position of the crack tip is observed visually and marked every 5 mm (positions marked on the sample) in the load-displacement curve. The curve recorded by the UTS shows the load as a function of the displacement.

3.3 Mode II delamination test

The test normally used for this mode is the ENF (end notched flexure) test:

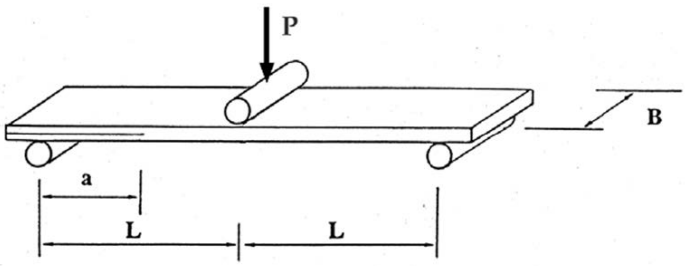

Figure 8: Configuration of the delamination test in mode II, with applied load P, crack length a, beam length $2L$, and width B.

Due to the unstable nature of the test geometry, this test will not be performed during the laboratory demonstration. The interested reader is referred to the bibliography for a more in-depth approach to the ENF test.

4 Questions

1. For the fix span case, calculate the elastic modulus of the composite laminate E_s and the flexural stiffness D of the beams using the Euler-Bernouilli beam theory. Compare the results you obtain using different calculation methods, e.g. slope of the load-displacement curve (equations 1 - 3), sandwich approximation (equation 6)

2. For the sandwich tested at different spans, use the shear-corrected beam deflection to calculate its flexural stiffness D and shear stiffness S. For this purpose, you can linearize equation 7 and obtain D and S through its slope and intercept:

$$\delta = \frac{L^3}{48D}P + \frac{L}{4S}P \Rightarrow \begin{cases} \frac{\delta}{PL^3} = \frac{1}{4S}L^{-2} + \frac{1}{48D} \\ \frac{\delta}{PL} = \frac{1}{48D}L^2 + \frac{1}{4S} \end{cases} \tag{14}$$

3. Compare the flexural stiffnesses you obtain in the previous two sections. Do they make sense? Discuss the influence of the span to depth ratio in the determination of the flexural rigidity with a three point-bending test, and relate it to the test you performed. You might want to read through the suggested bibliography.

4. Calculate the average energy release rate in mode I G_I (equation 13) with the data collected from the DCB test (do not forget that this geometry is different from the single cantilever case). In order to obtain the exponent n, you can take logarithms to

linearize equation 12 as a function of crack length and determine its slope:

$$\delta = \frac{a^n}{3EI}P \Rightarrow \ln\left(\frac{\delta}{P}\right) = n\ln(a) + \text{intercept} \tag{15}$$

What does the calculated value of your exponent mean?

Attention:

1. **For three point bending test, the UTM software record the displacement after reaching pre-load.**
2. **δ is equal to the crosshead displacement.**
3. **check the unit of all the data and results.**

Bibliography

1. P. Davies, *Influence of ENF Specimen Geometry and friction on the mode II Delamination Resistance of Carbon/PEEK*, Journal of Thermoplastic Composite Materials, 10, 1997.

2. W. O. W. Richardson, *Polymer Engineering Composites*, Applied Science Publishers Ltd, London, 212-220, 1977.

3. ASTM Standard Test Method for Mode I Interlaminar Fracture Toughness of Unidirectional Fiber-Reinforced Polymer Matrix Composites, D5528 – 13

4. ASTM Standard Test Method for Determination of the Mode II Interlaminar Fracture Toughness of Unidirectional Fiber-Reinforced Polymer Matrix Composites, D7905/D7905M – 14

Influence of ENF Specimen Geometry and Friction on the Mode II Delamination Resistance of Carbon/PEEK

P. DAVIES
Marine Materials Laboratory
IFREMER, Centre de Brest, BP 70
29280 Plouzané, France

ABSTRACT: Unidirectional carbon/polyetheretherketone (PEEK) composites were tested under mode II (shear) loading conditions. Three ENF (end notched flexure) specimen thicknesses have been tested, allowing a range of span length-to-thickness ratios to be examined. Analysis of the results from a first series of tests indicated a strong influence of specimen thickness on G_{IIc} values. However, a second series of tests was then performed on similar specimens under identical loading conditions but with a folded layer of PTFE film inserted between the crack faces to reduce friction. These test results were independent of specimen thickness except for the thickest specimens at the shortest span length. It is concluded that friction can cause overestimation of G_{IIc} values by up to 20%. A standard mode II test method must include steps to reduce this friction component.

INTRODUCTION

THERE IS CONSIDERABLE current interest in the measurement of reliable values of resistance to interlaminar crack propagation under mode II (forward in-plane shear) loading. Many structures are loaded in bending so defects are mainly subjected to shear. Compression-after-impact data has also been shown to correlate with mode II fracture toughness [1]. There is thus a need for interlaminar toughness data under this loading mode, to enable comparisons to be made between materials and to encourage the development of fracture-mechanics-based analyses. There is currently no widely accepted mode II standard test method, even though there are two commonly used test specimens. These are the ENF (end notched flexure), developed almost 20 years ago for testing wood [2], and the ELS (end loaded split) developed at Texas A&M University [3]. The latter has the advantage of stable crack propagation but requires a more complicated test fixture than the simple three-point-bend set-up required for the ENF test. Other specimen configurations have also been used for mode II testing [4]. The ASTM D30.06 sub-committee is running round-robin tests using the ENF specimen, for which a standard test method has been proposed by the JIS (Japanese Industrial Standards) group, JIS K 7086 [5]. The European

0892-7057/97/04 0353–09 $10.00/0
© 1997 Technomic Publishing Co., Inc.

Structural Integrity Society (ESIS) group is currently running tests on ENF and ELS specimens [6]. Two aspects of the mode II test have inspired considerable debate in recent years and have hindered the development of standard test methods, choice of defect type (film or precrack) to be used to start delaminations, and data analysis.

The choice of defect type has posed considerable difficulties in mode I testing. The ASTM mode I standard D5528 [7] specifies a film defect less than 13 μm thick, while the JIS mode I method [5] requires a mode I precrack unless a steep R-curve is detected. The philosophy behind the ASTM choice is that the minimum conservative value is sought, and this has been shown to correspond to non-precracked specimens [8]. The JIS approach, on the other hand, favors a natural precrack, as considerable problems have been encountered in obtaining satisfactory starter films. The latter may be wavy and can cause matrix-rich areas in front of the film. The problem is more complicated in mode II testing, as even thin starter films tend to produce higher G_{IIc} values than precracks [9].

The analysis of data from mode II tests has also been controversial and is discussed in Reference [4]. The small variation in specimen compliance with crack length makes experimental compliance calibration inaccurate, so it is necessary to rely on analytical solutions. A beam theory expression was developed [10] and later corrected for transverse shear [11] to provide the most commonly used data analysis. Much theoretical work was then performed, using finite element analysis and higher order plate theory, to check this expression.

Given the amount of work performed on analysis and the widespread use of the ENF specimen, remarkably little work has been performed to establish whether this test yields results that are independent of specimen geometry. Some results from an ESIS round-robin for carbon/PEEK composites, in which mode II delaminations were propagated from mode I precracks, showed an increase in G_{IIc} with increasing specimen thickness; it was suggested that this may have been a direct result of the precracking procedure [12]. Multiple cracking was noted in thicker specimens. Tests on carbon/epoxy specimens showed no influence of thickness on G_{IIc}. It was the main aim of the present work to examine this further, as carbon/PEEK specimens from the same batch of materials were available in three thicknesses. Varying the span length ($2L$) enabled a range of geometries to be investigated.

Finally, another aspect of this test that has not been fully explored experimentally is the influence of friction between the crack surfaces. Barrett and Foschi [2] suggested the use of a roller between the crack faces in wood specimens, and the ESIS protocols suggest using a PTFE film or a pencil lead. If a PTFE film is used as the starter insert, this may be expected to reduce friction at the contact points, but for high-temperature matrix composites other polymer films or aluminium foil are frequently employed as crack starters. Friction contributions were discussed by Carlsson et al. [11], and a non-dimensional expression for the influence of friction was presented:

$$\frac{G_{II}^{SH} - G_{II}^{SH}(\mu)}{G_{II}^{BT}} = \frac{4}{3}\mu\frac{h}{a} \tag{1}$$

with SH corresponding to the shear corrected beam theory (BT) expression given later [Equation (3)] and μ the coefficient of sliding friction. This indicates that for a given crack length the error in G_{IIc} due to friction should increase linearly with specimen thickness. Finite element analysis of typical specimen geometries with h/a less than 0.05 showed the error due to friction to be less than 2 to 5%.

MATERIALS AND TEST METHOD

The composite tested here is unidirectional carbon-fiber (AS4) reinforced PEEK (polyetheretherketone). The materials were supplied in the form of 12-, 24- and 40-ply panels by ICI Wilton, UK. Their thicknesses were nominally 1.6, 3.2 and 5.2 mm. Fiber volume fraction was close to 0.6. Single-sheet aluminum foil starter films coated with release agent were included at mid-thickness during molding. Their thickness was measured to be 20 to 25 μm. This is thicker than the film thickness specified in mode I standards (ASTM recommended less than 13 μm). Published results suggest that G_{IIc} values measured from 25-μm films in carbon/PEEK composites are larger than those from 13 or 6.5 micron films, which are in turn larger than those from precracks [8]. However, precracking introduces damage in front of the crack tip and was observed to produce multiple cracking in previous tests on these carbon/PEEK materials [12]. To enable evaluation of the influence of specimen geometry from similar starter defects, in this study all mode II tests were performed without precracking.

Panels were cut into 20-mm-wide strips for ENF testing (Figure 1), and all tests were performed under displacement control at 1 mm/min. Using the same crosshead displacement speed for different specimen geometries will result in differences in crack tip loading rates, but these were estimated not to be significant over the range tested. Load-displacement plots were recorded. Two series of tests were performed at span lengths ($2L$) of 60, 80, 100, 132 and 164 mm. All tests were performed with an a/L ratio of 0.5. For the first series no additional film separator was introduced between crack faces, while for the second series a thin folded layer of 25-μm thick PTFE film was placed between the starter crack surfaces at the specimen end above the outer load point. In total, 63 tests were performed (Table 1).

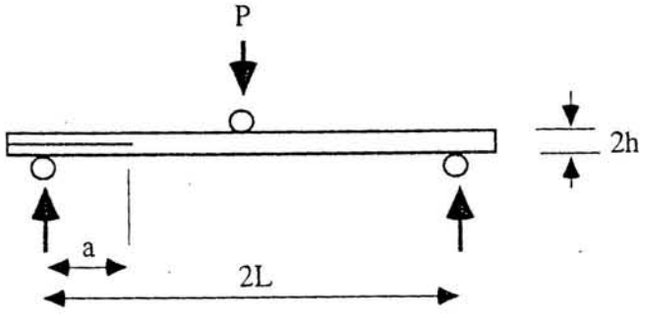

Figure 1. *Specimen configuration.*

Table 1. Number of specimens tested.

	Without PTFE			With PTFE		
2L (mm)	1.6 mm	3.2 mm	5.2 mm	1.6 mm	3.2 mm	5.2 mm
60	3	4	3	5	3	3
80	—	—	4	—	3	5
100	—	2	3	—	3	6
130	—	—	3	—	3	4
164	—	—	3	—	—	3

Data were analyzed using the following beam theory expression derived by Russell and Street [10]:

$$G_{II} = \frac{9P\delta a^2}{2B(2L^3 + 3a^3)} \tag{2}$$

with P the load, δ the displacement, a the crack length, B the specimen width, and L half the span length. Other expressions are available requiring moduli values or an experimental compliance calibration [3–5]. However, the aim of the present study was not to evaluate data reduction methods but simply to compare results from different specimen geometries on a consistent basis. Large displacement corrections were calculated using the expressions derived by Williams [13], but the largest correction necessary was 3%. Transverse shear corrections were also applied, using the expression presented by Carlsson et al. below [11]:

$$G_{II}^{SH} = G_{II}(1 + S) \tag{3}$$

where

$$S = 0.2\left(\frac{E_1}{G_{13}}\right)\frac{h^2}{a^2}$$

taking values of E_1 and G_{13} as 134 and 5.1 GPa, respectively. This correction reached nearly 20% for the thickest specimens at the shortest span.

Two critical load-displacement combinations, corresponding to the deviation from linearity on the load-displacement plot (NL) and the maximum load which immediately preceded unstable crack propagation, were used in the analysis as shown in Figure 2. These combinations yield critical strain energy release rate values of G_{IINL} and G_{IIc} respectively.

RESULTS AND DISCUSSION

For the test conditions where four or more specimens were tested, the coefficients of variation ranged from 5 to 20% for G_{IINL} and G_{IIc}, with more scatter for

maximum load values. The mode II toughnesses from the first series of tests without a PTFE film separator between the crack surfaces are shown versus span length in Figure 3. The results for the two specimen thicknesses do not superpose, regardless of whether G_{IINL} or G_{IIc} is considered, and thicker specimens give higher values. Values of G_{IINL} and G_{IIc} increase with decreasing span length. It may be that at shorter span lengths, there is increasing crack tip interaction with regions of the specimen affected by the contact stress field caused by load introduction at the center load point, although Carlsson et al. [14] estimated that the affected length is equal to only one specimen thickness on each side of the loading nose.

The results from the second series of tests, with a film separator, are shown in Figure 4. Here the values for the 5.2-mm-thick specimens are considerably lower and are close to those for the 3.2-mm-thick specimens over most of the range except for the shortest span length ($2L = 60$ mm). For this distance it may be that indentation effects or crack tip interaction with the load point stress field are influencing measured values. For the 5.2-mm-thick specimens, the displacements measured at non-linearity and maximum load are small (less than 1.5 mm). The insertion of a PTFE film reduced the G_{IIc} and G_{IINL} values for the stiffest specimens by about 20%. This is shown more clearly for the G_{IINL} values for the 5.2-

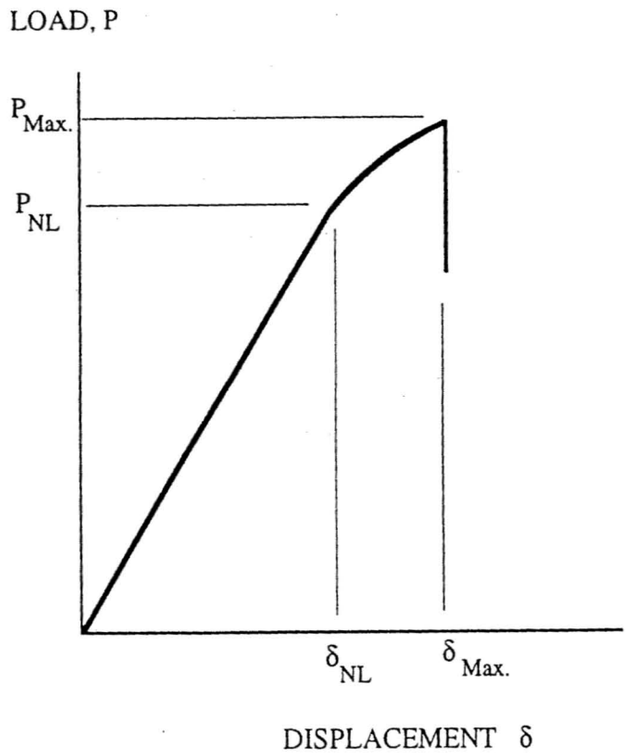

Figure 2. *Load-displacement plot.*

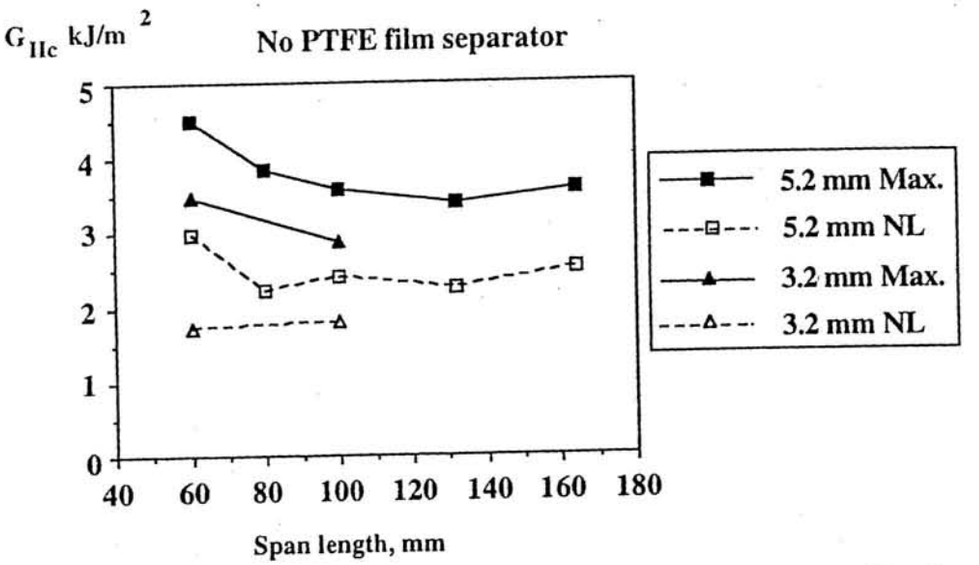

Figure 3. Results from mode II tests without PTFE film separator versus span length.

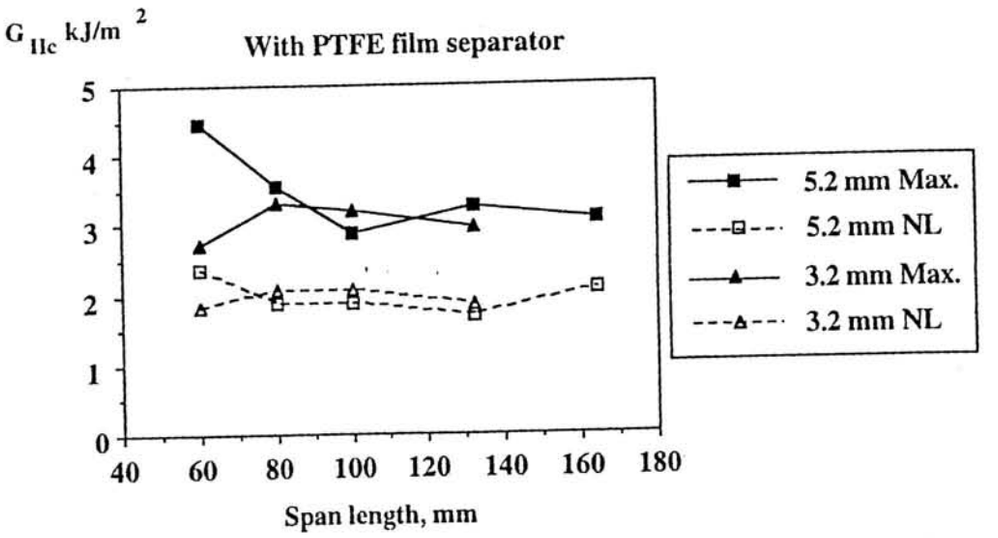

Figure 4. Results from mode II tests with PTFE film separator versus span length.

mm specimen thickness in Figure 5. Fewer tests were performed on the 3.2-mm-thick specimens than on those of 5.2-mm thickness, so it is more difficult to establish the influence of the film separator. For tests performed with the film separator, the values of G_{IINL} and G_{IIc} are reasonably independent of specimen geometry over a range covering the most commonly used thickness and span length combinations. These are typically $2L = 100$ mm for a specimen thickness of 3 mm or greater. The values of G_{IINL} vary less than G_{IIc}. The latter will depend on the degree of non-linearity of the curves which was slightly higher for the 5 mm/60 mm combination, but no consistent trend with L/h was apparent. For all but one specimen, the degree of non-linearity, i.e., the difference between initial compliance and compliance at maximum load, was less than 10%.

All mean values of G_{IINL} and G_{IIc} are listed in Table 2. These values are larger than those measured from mode I precracks measured on this same batch of material [12], even with the PTFE film separator, which indicates that the 20–25 μm starter film used here is too blunt to simulate a natural crack.

CONCLUSION

The experimental results presented in this paper indicate that the values of G_{IINL} and G_{IIc} measured using the ENF specimen, with crack-length-to-span-length ratio of 0.5, are independent of geometry, *provided that a PTFE film separator is placed between the crack surfaces and that the span-length-to-specimen-thickness ratio is greater than 20.* If no film separator is used, friction can cause

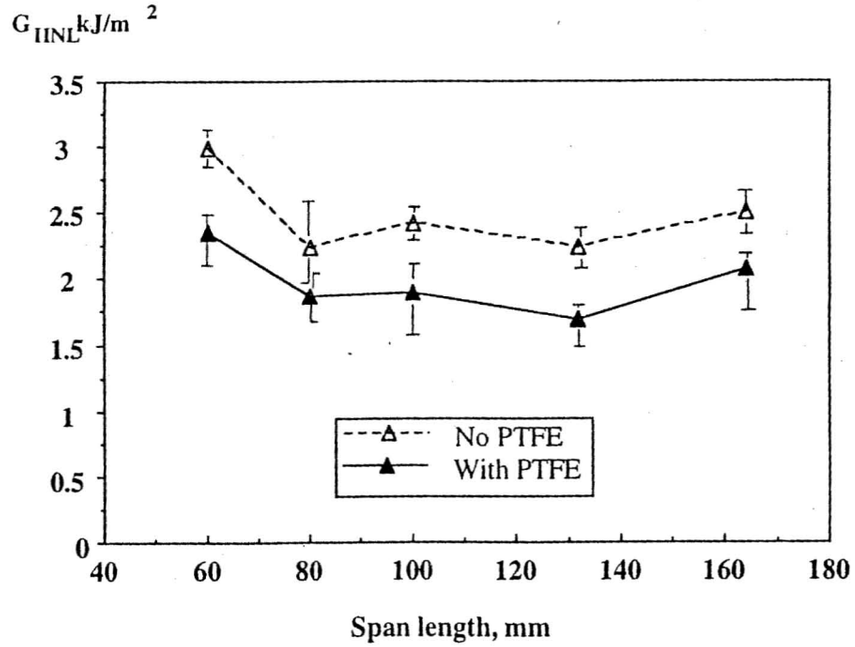

Figure 5. *Results for G_{IINL} from mode II tests on 5.2-mm-thick specimens, with and without PTFE separator. Error bars show maximum and minimum values measured.*

Table 2. Mean values of G_{IINL} (upper) and G_{IIc} (lower), kJ/m².

	Without PTFE			With PTFE		
2*L* (mm)	1.6 mm	3.2 mm	5.2 mm	1.6 mm	3.2 mm	5.2 mm
60	1.55	1.73	2.99	1.62	1.82	2.35
	2.82	3.49	4.51	2.51	2.72	4.47
80	—	—	2.24	—	2.07	1.87
	—	—	3.85	—	3.30	3.55
100	—	1.80	2.42	—	2.07	1.89
	—	2.87	3.58	—	3.20	2.87
132	—	—	2.24	—	1.85	1.69
	—	—	3.39	—	2.95	3.26
164	—	—	2.51	—	—	2.08
	—	—	3.60	—	—	3.06

an overestimation of fracture toughnesses by up to 20% for thick specimens. This is much higher than numerical estimations of the effect of friction reported previously and must be considered in the development of a standard mode II test method. It is suggested that when the starter film itself is not PTFE (i.e., another polymer or aluminum), the use of PTFE spacers between crack faces be made obligatory for these tests to minimize specimen geometry dependence.

ACKNOWLEDGEMENTS

The gift of materials from Dr. Roy Moore, ICI Wilton, UK is gratefully acknowledged.

REFERENCES

1. Masters, J. E. 1987. "Correlation of Impact and Delamination Resistance in Interleafed Laminates," *Proc. ICCM6/ECCM2*, London, Elsevier Vol. 3, p. 96.
2. Barrett, J. D. and R. O. Foschi. 1977. "Mode II Stress Intensity Factors for Cracked Wood Beams," *Eng Fract. Mech.*, 9:371.
3. Vanderkley, P. S. 1981. "Mode I–Mode II Delamination Fracture Toughness of a Unidirectional Graphite/Epoxy Composite," M.Sc. thesis, Mech. Eng., Texas A&M Univ.
4. Carlsson, L. A. and J. W. Gillespie, Jr. 1989. "Mode-II Interlaminar Fracture of Composites," Chapter 4 in *Application of Fracture Mechanics to Composite Materials*, ed., K. Friedrich, Elsevier.
5. Japanese Industrial Standard JIS K 7086. 1993. "Testing Methods for Interlaminar Fracture Toughness of Carbon Fibre Reinforced Plastics."
6. European Structural Integrity Society (ESIS) Protocols for Interlaminar Fracture Testing, Mode I (DCB), Mode II (ENF & ELS), Mixed Mode I/II (ADCB), 1st version November 1988 (latest version available from the author).

7. *ASTM D5528-94a.* 1994. "Standard Test Method for Mode I Interlaminar Fracture Toughness of Unidirectional Fiber-Reinforced Polymer Matrix Composites."
8. Davies, P., W. J. Cantwell and H. H. Kausch. 1989. "Measurement of Initiation Values of G_{Ic} in IM6/PEEK Composites," *Compos. Sci. & Tech.*, 35:301.
9. Davies, P., W. J. Cantwell and H. H. Kausch. 1990. "Delamination from Thin Starter Films in Carbon Fibre/PEEK Composites," *J. Mater. Sci. Letters*, 9:1349–1350.
10. Russell, A. J. and K. N. Street. 1982. "Factors Affecting the Interlaminar Fracture Energy of Graphite/Epoxy Laminates," *Proc. ICCM-IV*, Tokyo, p. 279.
11. Carlsson, L. A., J. W. Gillespie, Jr. and R. B. Pipes. 1986. "On the Analysis and Design of the End Notched Flexure Specimen for Mode II Testing," *J. Compos. Mats.*, 20:594.
12. Davies, P. et al. 1992. "Round Robin Interlaminar Fracture Testing of Carbon Fibre Reinforced Epoxy and PEEK Composites," *Compos. Sci. & Tech.*, 43:129.
13. Hashemi, S., A. J. Kinloch and J. G. Williams. 1990. "The Analysis of Interlaminar Fracture in Uniaxial Fibre-Polymer Composites," *Proc. Royal Soc.*, A427:173.
14. Carlsson, L. A., J. W. Gillespie, Jr. and B. R. Trethewey. 1987. "Finite Element and Plate Theory Based Design and Data Reduction of the ENF Specimen," *Proc. Am. Soc. for Compos., 2nd Conf. on Compos. Materials*, Technomic Publishing Co., Inc., Lancaster, PA, p. 399.

M. O. W. Richardson, Polymer Engineering Composites, Applied Science Publishers Ltd, London, p. 212-220, 1977.

4.6 SHORTCOMINGS OF THE LAW OF MIXTURES IN BEND FOR LAMINATED COMPOSITES

When, as in laminated composites, the modulus varies through the cross-section, according to the different constituent layers, the simple theory of

bending, with its assumption of homogeneity, is no longer valid. The outer layers being strained to a greater degree than the inner layers during bending have greater influence on the bending moment at a given curvature, *i.e.* on the stiffness.

If the outer layer or layers consists of relatively low modulus material, as in the case of a gelcoat on a GRP sheet, the modulus in bend will be slightly lowered as compared with the modulus of the same sheet in tension, when all layers are strained equally. This is the reason for the difference between theoretical bend and tensile moduli in Fig. 5, just discussed, where the sheets were all gelcoated. Such cases of 2-layer laminates can be treated theoretically by an extension to the law of mixtures as shown later.

A much more distinctive class of laminated composites are the sandwich constructions in which high bending stiffness is obtained by the use of thin skins of a stiff material as outer layers bonded to a thick but low modulus core. Such constructions have been extensively developed for the aircraft industry where the combination of thin metal faces spread apart by a core of honeycomb or other low density material results in extremely rigid but light structures. The same form of construction is also applied in building panels and boat building, where the skins are frequently of GRP and the cores of balsa wood or foamed plastic. In all these applications the main function of the core is to space the stiff material, namely the skins, away from the central plane, the neutral axis in bending, so as to make their stiffening effect greater. This is the same principle as stiffening a plate by means of ribs or flanges as is the usual practice with GRP boat hulls of single skin construction.

The theory of sandwich construction from an engineering standpoint is fully treated by H. G. Allen.[8] It will suffice here to give an elementary theory of flexural stiffness of a symmetrical sandwich construction, *i.e.* one with skins of equal thickness.

4.7 STIFFNESS OF SANDWICH CONSTRUCTIONS

4.7.1 Elementary theory

Consider a sandwich construction consisting of two skins of thickness t, modulus E_s, and a core of thickness c, modulus E_c (as shown in section in Fig. 6).

The flexural rigidity (D) of the combination is the sum of the values EI for the individual layers about the neutral axis, namely $2E_sI_s + E_cI_c$ where I_s and I_c are the second moments of the area of the cross-section of each skin

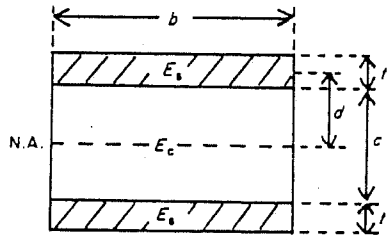

Fig. 6 Cross-section of sandwich construction.

and the core respectively, about the neutral axis. Since this is a symmetrical structure with equal skins on each side, the neutral axis must be central.

The second moment for the core about its own central plane (which coincides with the neutral axis) is

$$I_c = \frac{bc^3}{12}$$

where b is the width of the section being considered.

The second moment for each skin about its own centre line is

$$\frac{bt^3}{12}$$

and about the neutral axis is

$$I_s = \frac{bt^3}{12} + btd^2$$

where d is the distance from the centre line of each skin to the neutral axis.

Hence

$$D = 2E_sI_s + E_cI_c$$

$$= E_s\left(\frac{bt^3}{6} + 2btd^2\right) + \frac{E_cbc^3}{12}$$

When the skin thickness is small compared with the core thickness, $t^2 \ll d^2$ and the first term $(bt^3/6)$ can be ignored in comparison with the second $(2btd^2)$. Also when the core is a very low modulus material, as is usually the case, the final term $E_cbc^3/12$ can likewise be ignored. Hence $D \sim 2E_sbtd^2$.

4.7.2 Example

As an example, consider a sandwich construction employing two GRP skins each 3 mm thick made from CSM-reinforced polyester resin, in combination with a polyurethane foam core 24 mm thick. Suppose it to be in the form of a narrow beam 100 mm wide.

Typical modulus values for CSM polyester sheet and polyurethane foam are $E_s = 7000\ \text{N/mm}^2$ and $E_c = 20\ \text{N/mm}^2$ respectively.

Now $t = 3$ mm, $c = 24$ mm and $b = 100$ mm. Hence

$$d = \frac{t + c}{2} = \frac{27}{2} = 13{\cdot}5\ \text{mm}$$

$\therefore$ Flexural rigidity

$$D = E_s\left(\frac{bt^3}{6} + 2btd^2\right) + \frac{E_cbc^3}{12}$$

$$= 7000(450 + 109\,350) + 2\,304\,000$$

$$= (3150 + 765\,450 + 2304) \times 10^3$$

$$= 771 \times 10^6\ \text{Nmm}^2$$

[Note that the approximation $D \sim 2E_sbtd^2$ gives the value $765 \times 10^6\ \text{Nmm}^2$ which is in error by less than 1% in this case.] It is of interest to compare the flexural rigidity of this sandwich construction beam with the flexural rigidity of the GRP skins alone, supposing these not to be separated but to consist of a single layer of 6 mm thickness.

$$\text{Flexural rigidity of 6 mm thick GRP} = \frac{E_sbt^3}{12} \qquad \text{where } t = 6\ \text{mm}$$

$$= 12{\cdot}6 \times 10^6\ \text{Nmm}^2$$

The flexural rigidity of the GRP sheet is therefore increased by $771/12{\cdot}6 = 61$ times simply by splitting it and spacing the halves apart with a 24 mm core of very low modulus material. The tensile stiffness would however be practically unaffected.

4.7.3 'Modulus' of sandwich constructions

Having derived an expression for the stiffness in bend (flexural rigidity) of a sandwich construction it is tempting to calculate a bend 'modulus' analogous to that of a single homogeneous material, by dividing the flexural rigidity D by the second moment of area of the complete cross-section, that is by $bt^3/12$ where t is now the overall thickness of skins and core.

While a 'modulus' calculated in this way may ease the comparison of the properties of one type of sandwich construction with another or with a homogeneous composite by making allowance for differences in their

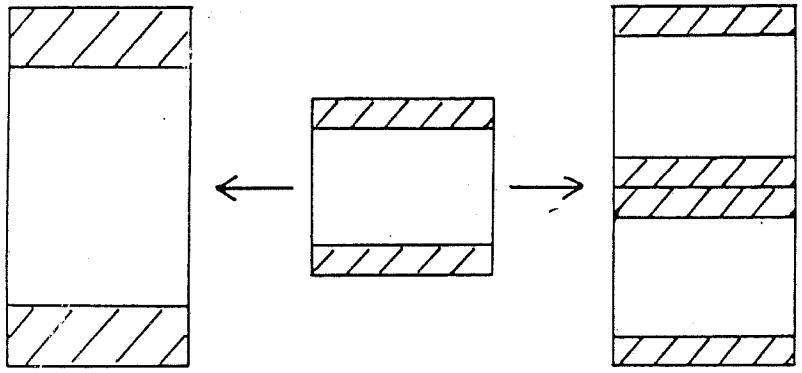

Fig. 7 Two methods of doubling a sandwich construction showing resultant differences in flexural rigidity and 'modulus'.

overall thickness, the figure so obtained is easily misunderstood or misapplied. For example, by bonding together two identical sandwich constructions, so as to double the overall thickness, the stiffness in bend will not be increased 8 times as it would be for a homogeneous material. In theory it would be increased only about 4 times and the 'modulus' would be about halved (see RHS of Fig. 7).

Only by doubling both skin and core thickness, while retaining the same form of construction (LHS of diagram) will the stiffness be increased 8 times and the 'modulus' remain the same. This shows the arbitrary nature of a 'modulus' calculated from a laminated structure and its comparative uselessness for forecasting the stiffness of other structures based on the same unit. Calculations of 'modulus' of sandwich structures and laminated composites in general are therefore best avoided (or, at the very least, to be examined very very carefully and critically).

4.7.4 'Stiffness at a given weight' in sandwich constructions

As mentioned previously, the stiffness at a given weight of a composite material or structure is of great importance in some applications and especially in aircraft construction where the economic advantages of reduced weight, and thereby increased payload, are obvious.

In the case of sandwich constructions, as with glass fibre/polyester composites, it has been found that there is an optimum proportion of the

two component materials giving maximum stiffness at a given total weight per unit area. Provided that the skins are thin compared with the core, this optimum occurs when the combined weight per unit area of the skins is one third of the total weight of skins plus core. H. G. Allen[8] gives a proof of this based on an earlier publication by E. W. Kuenzi[9] so it will not be repeated here.

As an example of the optimisation process, consider again the sandwich construction discussed earlier in section 4.7.2.

This had 2 GRP skins each 3 mm thick and a polyurethane foam core 24 mm thick.

Assume that skins and core had typical density values of 1·47 and 0·08 g/cm^3 respectively.

Then the weight per unit area of each skin $= 3 \times 1{\cdot}47 \times 10^3 = 4410$ g/m^2, weight per unit area of 2 skins $= 2 \times 4410 = 8820$ g/m^2 and weight per unit area of core $= 24 \times 0{\cdot}08 \times 10^3 = 1920$ g/m^2. Total weight per unit area of sandwich construction $= 8820 + 1920 = 10\,740$ g/m^2. The combined weight of the skins at 8820 g/m^2 is clearly much above the optimum of one third of the total weight, namely $10\,740/3 = 3580$ g/m^2.

The maximum flexural rigidity obtained at the total weight of 10 740 g/m^2 may now be calculated, taking 3580 g/m^2 as the combined weight of the 2 skins and $(10\,740 - 3580) = 7160$ g/m^2 as the weight of the core.

Thickness of each skin,

$$t = \frac{3580}{2} \times \frac{1}{1{\cdot}47 \times 10^3} = 1{\cdot}22 \text{ mm}$$

Thickness of core,

$$c = 7160 \times \frac{1}{0{\cdot}08 \times 10^3} = 89{\cdot}5 \text{ mm}$$

Using these values for t and c in place of 3 and 24 mm respectively in the previous calculation of flexural rigidity leads to the value

$$D = 3630 \times 10^6 \text{ Nmm}^2$$

This optimum flexural rigidity is nearly 5 times the value 771×10^6 obtained with the previous, less efficient, balance between skin and core weights. The fact that these calculations based on the weight fraction of one third for the skins, do forecast the optimum very accurately, can be seen from Fig. 8 which is a plot of flexural rigidity D against skin thickness for the case just examined, namely a total weight of 10 740 g/m^2.

The maximum of 3620 MNmm^2 approximately does occur at 1·22 mm skin thickness as accurately as can be read from the graph. The relatively

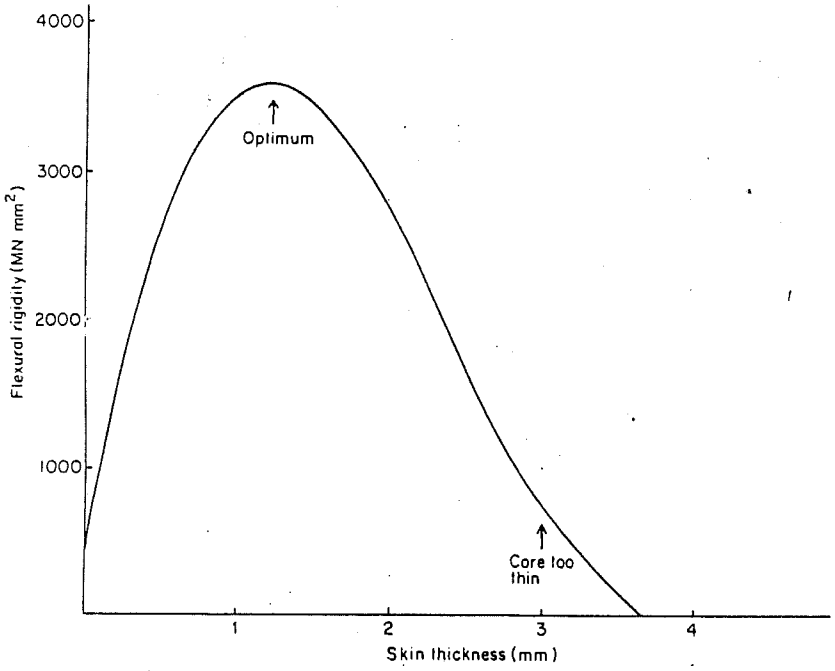

Fig. 8 Flexural rigidity as a function of skin thickness for a sandwich construction of fixed weight per unit area, showing an optimum skin thickness.

poor stiffness of $771 \times 10^6 \text{Nmm}^2$ previously obtained with a skin thickness of 3 mm is also seen. This corresponds with a thickness of core much below the optimum and the small spacing of the skins away from the neutral axis accounts mainly for the low stiffness.

It is not necessarily practical to optimise the flexural rigidity in the way just described, because skin and core materials may not be available in the particular thicknesses needed or because other requirements, for example, resistance to impact, may dictate thicker skins. Also, as will be shown in the next section, the deflection of a sandwich construction under transverse load may, with some core materials, be due as much, if not more, to shearing of the core material as to extension and compression of the skins, *i.e.* to pure bending as measured by the flexural rigidity.

4.7.5 Core shear in sandwich constructions

In the above theoretical treatment of the bending of sandwich constructions

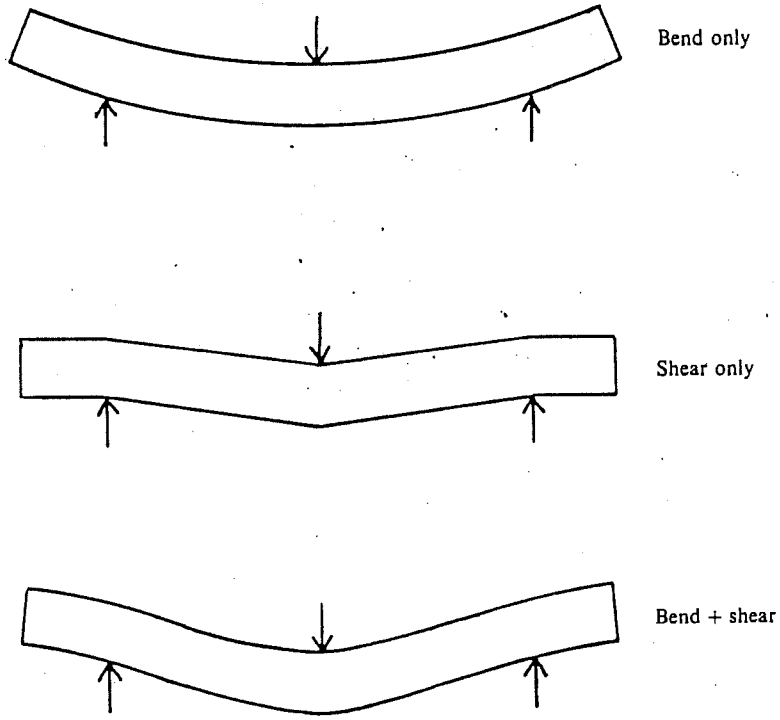

Fig. 9 Bending and shearing in 3-point loading of a sandwich construction.

it has been assumed that the construction is subjected to a pure bending moment and is free from shear stresses. Most bending situations however arise from transverse loads which give rise to shear stresses and, in these conditions, appreciable shear deformation of the core is likely to occur when this is a relatively soft material, as is often the case. Thus shear deflection adds to the bending deflection of a sandwich construction beam in 3-point loading as illustrated in Fig. 9.

Shear deflection becomes a smaller proportion of the total deflection as the span increases. This is because the bending deflection increases as the cube of the span and therefore much more rapidly than the shear deflection which only increases as the first power of the span. With soft core materials measurement of flexural rigidity is in error due to shear deflection at low span to depth ratios such as 16:1 which are satisfactory for homogeneous materials. To be reasonably free from shear, flexural rigidity measurements on sandwich constructions need to be made at very high span to depth

ratios. Values such as 48:1 minimum have been recommended and even higher values are probably necessary with very flexible cores such as some types of plastic foam.

The effect of shear at low span to depth ratios is shown in Table 6, which gives the results of 3-point bend tests at 10:1 and 20:1 span to depth ratios on two sandwich constructions made from different core materials but with similar skins (CSM-reinforced polyester resin) and of similar cross-sections.

TABLE 6
FLEXURAL RIGIDITY OF TWO SANDWICH CONSTRUCTIONS AT DIFFERENT SPAN TO DEPTH RATIOS

	Span to depth ratio		
Core material	10:1	20:1	*Very large*
Polyurethane foam	30	100	†420 MNmm^2
End-grain balsa wood	210	300	†340 MNmm^2

† Estimated values.

There is a drop in the measured value due to shear at the 10:1 level of span to depth ratio compared to 20:1 but the drop is very much greater with the foam core. The fact that core shear deformation was occurring during these tests even at 20:1 was very evident from the shape assumed by the foam-cored specimen while under load which resembled the third of the diagrams in Fig. 9 rather than the first.

The size of available specimens and apparatus often limits the span to depth ratio that can be employed in testing, so that a ratio large enough to avoid shear is usually not practicable. However when tests are carried out at two different span to depth ratios it is possible to estimate the flexural deflection separately from the shear deflection and in this way to calculate a flexural rigidity uninfluenced by shear. The figures presented in the last column of Table 6 were estimated in this way. The method involves the solution of simultaneous equations for the total deflection due to bending and shearing at the two spans, on the lines suggested in Ref. 10.

This analysis showed that, in the worst case, *i.e.* the foam core at 10:1 span to depth ratio, the deflection due to shear was about 12 times that due to bending. In the best case, *i.e.* the balsa wood core at 20:1 span to depth ratio, the shear deflection was only $\frac{1}{7}$ (15%) of the bending deflection. The implications of core shear deformations in the calculation of stresses, deflections and buckling loads are discussed by H. G. Allen in Ref. 11.